Okhotsk Sea and Polar Oceans Research 8 (2024) 17-23

https://doi.org/10.57287/ospor.8.17

Article

Laboratory experiments on spray icing with urea-doped water using flat and cylindrical specimens

Toshihiro OZEKI[1], Takatoshi MATSUZAWA[2], Shingo NOMURA[1], Satoru ADACHI[3], Taiki TOKUDOME[4] and Akihisa KONNO[4]

[1]*Hokkaido University of Education Sapporo, Sapporo, Japan*
[2]*National Maritime Research Institute, Mitaka, Japan*
[3]*Snow and Ice Research Center, National Institute of Earth Science and Disaster Resilience, Shinjo, Japan*
[4]*Kogakuin University, Hachioji, Japan*

(Received November 17, 2023; Revised manuscript accepted January 26, 2024)

Abstract

Urea-doped spray icing experiments were carried out on flat-plate and cylindrical specimens. The cylindrical specimens were tested at different diameters and the flat-plate was set directly facing the wind direction. Two wind speeds and three spray particle sizes were used. In the tests with diameters of 165 and 520 mm Φ, approximately half of the impinging sprays froze; for the 60 mm Φ, the icing rate was clearly greater than 50 %. This result suggests that the effect of diameter on the icing rate per impinging water varies between diameters of 60 mm Φ and 165 mm Φ. The amount of icing weight per unit time unit cross section increased with decreasing diameter. On the other hand, the increase in icing cross sectional area obtained from the graphical data analysis was greater for cylinders with a diameter of 520 mm and smaller for cylinders with a diameter of 165 mm. This result suggests that the horizontal cross-section of the icing growing on the specimen deviates from an elliptical shape as the diameter decreases. The icing rate of the flat plate is plotted as a function of its width, i.e. 1000 mm. The coefficient of determination for the logarithmic approximation is 0.77, which is in good agreement.

Key words: marine icing, spray icing, urea-doped water, wet growth, brine

1. Introduction

In recent years, the sea ice conditions of the Arctic Ocean have been changing annually and they will undergo further changes as global warming intensifies. As the open water area of the Arctic Sea route expands, the frequency of ships navigating that route will also increase. In the future, vessels with lower ice class and larger vessels will increasingly navigate. Marine icing will be an important factor in evaluating operational safety for vessels operating in weather and sea conditions where icing occurs.

Several researchers have simulated seawater spray icing growth. Makkonen (1987) developed a theoretical model of salt entrapment in spray ice. He assumed an analogy with sponginess of freshwater ice in wet growth. Lozowski *et al*. (2000) reviewed computer simulations of marine ice accretion and discussed the U. S. Coast Guard's Cutter Midgett model and a three-dimensional time-dependent vessel-icing model. Kulyakhtin and Tsarau (2014) applied a time-dependence model, MARICE, to the prediction of marine icing. MARICE calculated the turbulent airflow, trajectories of the droplets around the complete geometry of the structure, and heat transfer from the structure. Dehghani *et al*. (2017) and Dehghani *et al*.（2018）studied the water breakup phenomena of wave impact sea spray and developed a three-dimensional model for calculating the movement of a cloud of wave-impact sea spray over a Medium-sized Fishing Vessel (MFV). The results of spray impingement on the front side of the superstructure showed that 70 % of the droplets are smaller than 2 mm and 30 % are between 2 and 4 mm.

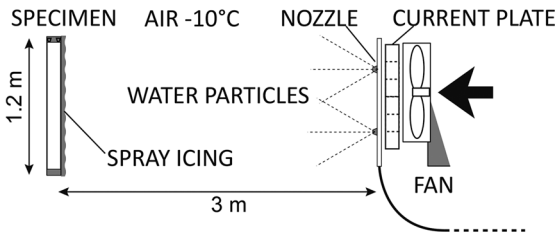

Fig. 1 A schematic view of experimental setting.

Because the phenomenon of sea spray icing is complex and the growth of icing varies depending on the shape of the ship and its superstructure, the practical risk of icing has been evaluated based on a relatively simple empirical equation *PR* (Overland, 1990) as following,

$$PR = \frac{V_a(T_f - T_a)}{1+0.4(T_w - T_f)}, \quad (1)$$

where *PR* is the predictor relating to icing rate, T_f is freezing point of seawater [°C], T_a is air temperature [°C], T_w is sea temperature [°C], V_a is wind speed [m s^{-1}]. The factor used to estimate the severity of potential spray icing is derived from a simplified heat balance of the icing surface, which do not consider the characteristics of individual ships or the availability of anti-icing measures.

Although the *PR* values are useful for evaluating the safety of icing during navigation, more information is needed to use them in ship design and operational planning. In this study, to obtain data that will contribute to the improvement of the *PR* equation, urea-doped spray icing experiment was conducted using a simple model of superstructure members.

2. Method of laboratory experiments

2.1 Equipment for spray icing experiments

The experimental apparatus (Fig. 1) was set up on an ice tank (20 m in length × 6 m in width × 1.8 m in depth) at the Technical Research Center of Japan Marine United Inc. The use of salt water is not permitted in this facility. The model ice for the ice tank test is made with urea-doped water so that brine is contained inside the ice. Therefore, we studied the icing characteristics of urea-doped water droplet icing including brine using a simple-shaped specimen.

Two fan-shaped nozzles (VE115-31 or VE115-59, Ikeuchi) and four fan-shaped nozzles (VP115-04, Ikeuchi) were installed on both sides of the fan, so that the sprayed water droplets were supplied to the specimen by the wind. The room temperature in the cold room was controlled at -10 ºC, and urea water with a concentration of about 20 ‰ was sprayed to grow brine-containing ice on the specimen.

In this study, PVC cylindrical specimens were tested at different diameters of 520 mm, 165 mm or 60 mm and a height of 1.2 m (Fig. 2). Experiments on flat plate (1000 mm in length × 918 mm in height) were carried out as well. The flat-plate specimen, painted with blue marine paint, was fixed on a dolly facing the wind direction (Fig. 2). The distribution of wind velocity and droplet impact around the specimen was measured separately prior to each icing experiment. Spray particle counter (SPC-S7, Niigata Denki) was used to measure the particle size distribution of the droplets.

2.2 Visualization of brine structure in urea-doped spray ice using X-ray CT and MRI

Recently, X-ray computerized tomography (CT) has been used to measure the three-dimensional distribution of brine inside the sea ice nondestructively (Kawamura, 1988; Obbard *et al*., 2009). Nuclear magnetic resonance (NMR) is compatible with brine and has been applied to the measurement of sea ice (Calaghan *et al*., 1999). In addition, magnetic resonance imaging (MRI) can acquire contrasting images in brine and ice mixtures (Edelstein and Schulson, 1991; Eicken, 2000; Menzel *et al*., 2000). Ozeki *et al*. (2005) measured the three-dimensional microstructure of sea-water spray ice using the MRI technique and confirmed the presence of such a channelized network of brine in natural sea-water spray ice samples (Fig. 3). In this study, X-ray CT and MRI system set up in a cold room was used to visualize the brine in sodium chloride ice.

We used a μCT 35 system (SCANCO Medical) with a resolution of 1.75–72 μm for the X-ray CT. Meanwhile MRI was performed using a yokeless magnet with a field strength of 1.04 T (Adachi *et al*. 2009). A three-dimensional single spin-echo (3D-SE) sequence (image matrix = 256^3, voxel size = $(100\ \mu m)^3$) was used for 3D high-resolution imaging. Each X-ray CT data and MRI data was analyzed using ImageJ that was an open source image processing software.

Fig. 2 Flat-plate and cylindrical specimens. Diameters of cylindrical specimens (left) are 520 mm, 165 mm, or 60 mm.

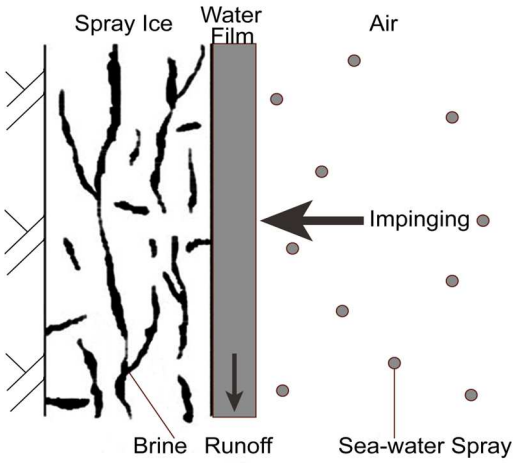

Fig. 3 A schematic vertical cross section of wet growth

Table 1. Specimen diameter and spray particle diameter (small droplet and very small droplet)

Diameter	VE115-31		VP115-04	
[mm]	10 m/s	7.5 m/s	10 m/s	7.5 m/s
60	#HS60	#MS60	#HV60	#MV60
165	#HS165	#MS165	#HV165	#MV165
520	#HS520	#MS520	#HV520	#MV520

Table 2. Nozzle model number for flat plate and corresponding cylindrical specimens.

Diameter	VE115-31	VE115-59
[mm]	10 m/s	10 m/s
Flat plate	#HSFlat	#HLFlat
60	#HS60	#HL60
165	#HS165	#HL165
520	#HS520	#HL520

3. Experimental results

3.1 Observation of spray ice and brine distribution

The icing test on the cylindrical specimens was conducted eighteen times with different specimen diameters, wind speeds and spray particle sizes. The test conditions and test numbers for small particles (VE115-31) and very small particles (VP115-04) are given in Table 1. In this experiment, the wind speed was about 10 m/s (high speed) or 7.5 m/s (middle speed) near the center of the specimen. The spraying was supplied continuously. The tests were conducted for 30 minutes each (20 minutes for #HS520 test), and the ice weight were measured at the end of each test at each one sixth height. The icing test on the flat plate specimen was conducted two times with small particles (VE115-31) and large particles (VE115-59) for 30 minutes each, and the wind speed was about 10 m/s near the center of the specimen. The ice weight was measured at the end of each test at each one forth height. The test conditions for the flat plate and corresponding cylindrical specimens test numbers are given in Table 2.

Spray particles impinging on the cylinder formed a water film, and part of the water froze into spongy ice as it flowed down the PVC surface. In the early stage, part of the spray ice peeled off and slide down the surface as slush. The spray ice was spongy and had a milky white color. This is consistent with the characteristics of ice containing brine. Therefore, urea-doped spray ice was expected to contain a high amount of brine.

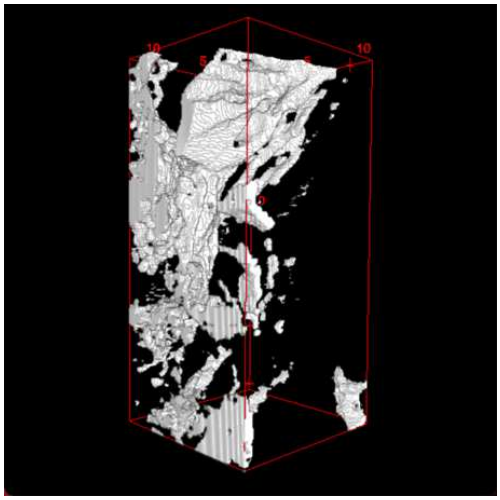

Fig. 4 Surface rendering of 3D X-ray image of brine distribution in spray ice created from 20‰ urea-doped spray water.

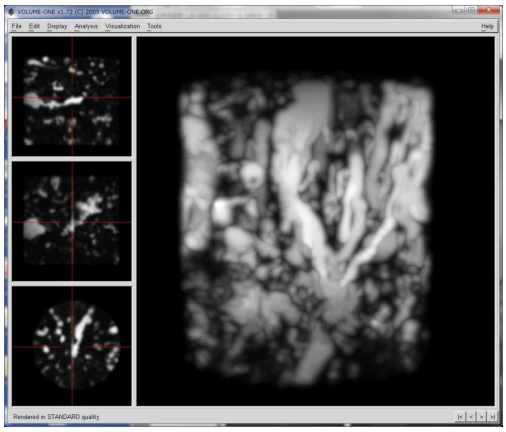

Fig. 5 3D MRI image of brine distribution in spray ice created from 30‰ sodium chloride spray water. (Ozeki *et al*., 2013)

Fig. 4 shows a 3D X-ray image of brine network of spray ice created from 20‰ urea-doped water spray. We used surface rendering to visualize the brine pockets and channels. We have confirmed that the urea-doped spray ice contains a high amount of brine, the bright regions in the figure. A vertically converging drainage channel was observed in the brine distribution in the spray ice.

Fig. 5 shows 3D MRI image of brine distribution in spray ice created from 30‰ sodium chloride spray water. Since the NMR signal from the ice was negligible as compared to that from the brine, the brine drainage channels appeared as bright regions. Left windows shows 2D slices selected from the 3D image data. Brine

drainage channels appear vertically in the sodium chloride spray ice. Structurally, urea-doped spray ice and sodium chloride spray ice were found to have very similar brine channels.

Fig.6 Cross-section area of the spray ice. Left: a PVC cylinder of 520mm diameter (#MV520), Right: difference between the trimming area including the spray ice and the projected area of specimen.

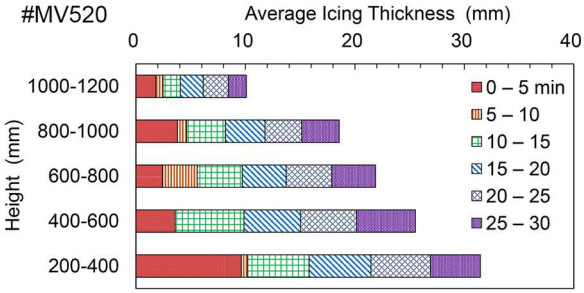

Fig. 7 Thickness of ice accretion every 5 minutes at every 20 cm height on a PVC cylinder of 520mm diameter (#MV520).

3.2. Graphic Data Processing

Projection area of ice accretion was obtained from graphic data set of each experiment (Fig. 6). In this study, the photographs were taken every minute from left side, and cropped to leave only the subjects that include ice accretion and the specimen. The cross-section area of the spray ice was obtained from the difference between the projected area of the trimming area including the spray ice and the projected area of specimen (Ozeki *et al*., 2022).

Fig. 7 shows the cross-sectional area of ice accretion every 5 minutes at every 20 cm height in test #MV520, and converted to the average thickness of ice accretion every 5 minutes at each height. The projected area of 0-200 mm included ice piled up from the floor and was

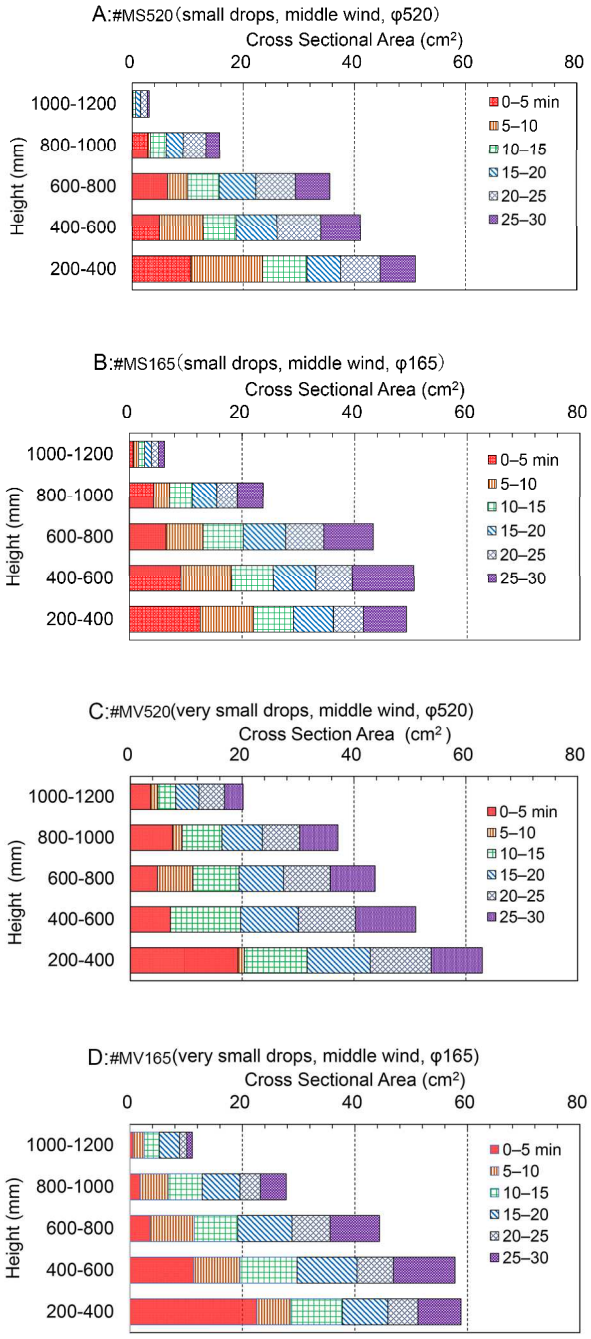

Fig. 8 Comparison of cross-sectional area of ice accretion every 5 minutes. A:#MS520, B:#MS165, C:#MV520, D:#MV165.

excluded from the analysis because it was difficult to separate ice accretion from ice on the floor. Focusing on the amount of growth during the first 5 minutes, the growth near the center of the cylinder (600-800 mm) was small. On the other hand, no growth was recorded at 400-600 mm in 5-10 min. This is because the sheet icing exfoliated and slide off. However, the growth became stable after that, and a distribution of thicker icing in the lower layers and thinner icing in the upper layers was formed after 30 minutes.

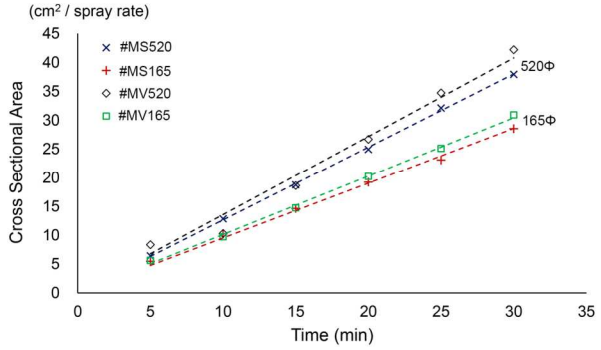

Fig. 9 Time series of cross-sectional area of ice accretion divided by the spray rate (kg m^{-2} min^{-1}) every 5 minutes.

Fig. 8 shows four graphs of the cross-sectional area of ice accretion every 5 minutes for tests #MS520 (Fig. 8A), #MS165 (Fig. 8B), #MV520 (Fig. 8C), and #MV165 (Fig. 8D) at heights of every 20 cm. In this figure, the cross-sectional area (cm^2), rather than the thickness of ice accretion (mm), was presented to comparison of each test. In the initial stage, there were differences in the vertical distribution of icing area depending on the diameter of the cylinder: for the specimens with 520 mm Φ (#MS520, #MV520), the area decreased once at 400-600 mm, while for the specimens with 165 mm Φ (#MS165, #MV165), the area monotonically increased toward the lower layers. However, after 30 minutes, the icing area in all specimens reached the distribution with thicker ice accretion in the lower layers and thinner ice accretion in the upper layers.

To compare the growth rate of icing on each test, the cross-sectional area of ice accretion was calculated every 5 minutes and divided by the spray rate (kg m^{-2} min^{-1}) for each test was plotted in Fig. 9. In all times, the cross-section increased linearly with time. The increasing rate was greater for the 520 mm diameter cylinder and smaller for the 165 mm cylinder. For the same diameter, the increasing rate for very small particles (#MV) was slightly greater than that for small particles (#MS).

3.3 Spray icing ratio

Table 3 shows the amount of spray water impinging on the specimen per unit time and unit area (*X*), and the amount of icing per unit time and unit area (*Y*); the projected area of the side surface of the specimen was used to calculate per unit area. Since the wind speed, projected area, and droplet particle size of each test were different, a direct comparison of the above values does not reveal a relationship. Therefore, the spray icing ratio *Y/X*, which represents the freezing rate relative to the impinging urea-doped water, was calculated. In both experiments on cylindrical specimens with diameters of

Table 3. Amount of spray water impinging on the specimen and amount of icing

Specimen	*X*: Spray Rate [kg m^{-2} min^{-1}]	*Y*: Ice Accretion [kg m^{-2} min^{-1}]	*Y/X*
#HS520	1.04	0.50	0.48
#MS520	0.64	0.31	0.48
#HV520	0.86	0.46	0.53
#MV520	0.85	0.39	0.46
#HS165	1.37	0.65	0.47
#MS165	1.01	0.57	0.56
#HV165	1.11	0.71	0.64
#MV165	1.18	0.58	0.49
#HS60	1.51	1.11	0.74
#MS60	1.16	1.09	0.94
#HV60	1.57	1.13	0.72
#MV60	no data	0.97	N/A

Table 4. Spray icing ratio (icing/impinging spray water) on the flat plate specimen and cylindrical specimens. Wind speed 10 m/s in center of specimens.

Diameter	VE115-31 Small particles	VE115-59 Large particles
Flat plate	0.34 (#HSFlat)	0.27 (#HLFlat)
60 mm Φ	0.74 (#HS60)	1.01 (#HL60)
165 mm Φ	0.47 (#HS165)	0.51 (#HL165)
520 mm Φ	0.48 (#HS520)	N/A (#HL520)

165 mm Φ and 520 mm Φ, approximately half of the impinging spray was frozen under these conditions, and there was no significant difference in the amount of ice formed over the entire sample per unit area. On the other hand, in the cylindrical specimen with a diameter of 60 mm Φ, *Y/X* was clearly larger than 50%, and the small particle test at 7.5 m/s (#MS60) showed a high value of 94%.

Table 4 shows the spray icing ratio for the flat plate specimen. The spray icing ratio for cylindrical specimens under the same test conditions was shown in the table. The small particle nozzle VE115-31 and the larger particle nozzle VE115-59 were used, however the heavier particles fell before they reached the specimens, and SPC measurements showed little difference in the particle size distributions of the two nozzles. The flat plate tended to have lower icing ratio than the cylindrical specimens. Moreover, the distribution of spray icing was concentrated on the edges.

Fig. 10 shows the spray icing ratio as a function of cylindrical specimen diameter. The flat plate does not correspond to a diameter, thus is plotted for a width of 1000 mm, which corresponds to the width of the flat plate. The spray icing ratio tended to decrease as the diameter increased. The coefficient of determination for the logarithmic approximation is 0.77, which is in good agreement.

4. Discussion

The increasing rate of the spray icing cross-sectional area was greater for the 520 mm Φ cylinder than for the

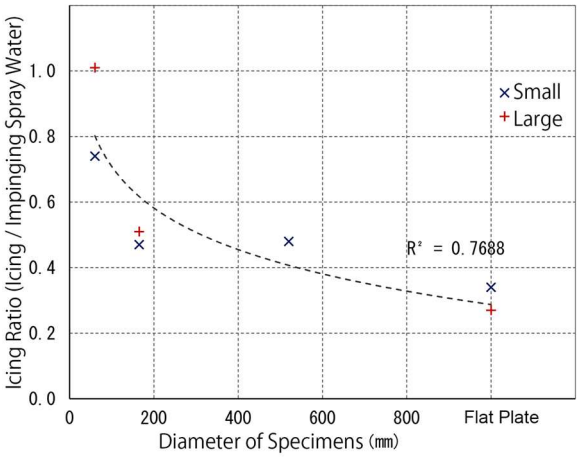

Fig. 10 Spray icing ratio as a function or the cylindrical specimen diameter. The flat plate is shown as equivalent to 1000 mm.

165mmΦ cylinder. On the other hand, the ratio of the amount of spray water impinging on the specimen (X) and the amount of spray icing (Y) was not significantly different between the spray icing ratio for 165 mmΦ and 520 mmΦ, with Y/X clearly larger for the 60 mmΦ cylinder. The difference between these two results is due to the difference in the horizontal cross-sectional shape of the spray icing.

Fig. 11 shows horizontal cross-sectional photographs of spray icing on 60 mm Φ, 165 mm Φ, and 520 mm Φ cylindrical specimens. The 520 mm Φ sample was thickest at the stagnation point on the windward front and became thinner toward the sides, while the 60 mm Φ sample had a shape where the edges protruded toward the sides. This is an expected result based on the trajectories of the streamlines and droplet particles. However, it is noteworthy that a change was observed between Φ165 mm and Φ60 mm. As a result, in the case of a thin cylinder, the icing grows significantly laterally, and its projected area become larger than the original projected area, which suggests that the amount of spray impinging the specimen was larger than the original.

5. Conclusion

Urea-doped spray icing experiment were conducted using a simple model of superstructure members. Twelve icing tests were conducted with different specimen diameters, wind speeds and spray particle sizes. After each test, ice weight and salinity were measured at each one-sixth height. In all tests of 165 mm Φ and 520mm Φ in diameter, approximately half of the impinging spray froze. On the other hand, in the tests using 60 mm Φ cylindrical specimen, frozen ratio was clearly larger than 50%. This result suggests that the effect of diameter on the icing rate per impinging water varies between diameters of 60 mm Φ and 165 mm Φ. The amount of icing weight per unit time unit cross section increased with decreasing diameter. On the other hand, the increase in icing cross sectional area obtained from the graphical data analysis was greater for cylinders with a diameter of 520 mm and smaller for cylinders with a diameter of 165 mm. This result suggests that the horizontal cross-section of the icing growing on the specimen deviates from an elliptical shape as the diameter decreases.

The experimental data will be useful for improving the PR equation by weighting the icing index according to the geometry of the object. Furthermore, as the development of icing is caused by the flight, collision, and freezing of wave spray particles, the icing index will be improved by estimating the trajectory of spray particles around the hull of a ship using CFD analysis.

Acknowledgment

We wish to express our gratitude to S. Mizuno, N. Nakazato and A. Maeda of JMU Technical Research Center. This work was supported by ArCSII JPMXD1420318865.

References

Adachi, S., T. Ozeki, R. Shigeki, S. Handa, K. Kose, T. Haishi, M. Aoki (2009): Development of a compact magnetic resonance imaging system for a cold room. *Rev. Sci. Instrum.*, **80**, Article 054701: doi.org/10.1063/1.3129362.

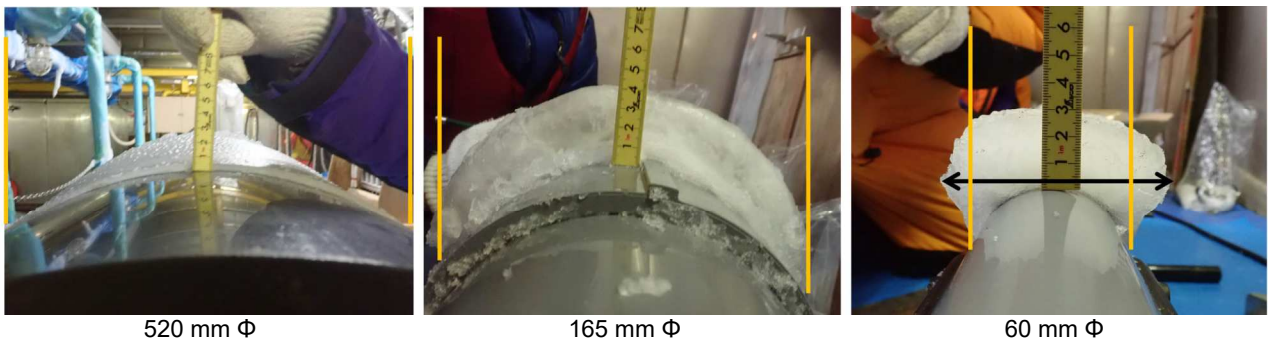

520 mm Φ 165 mm Φ 60 mm Φ

Fig. 11 Horizontal cross-sectional photographs of spray icing on 520 mm Φ, 165 mm Φ, and 60 mm Φ cylinders. The yellow reference line represents the icing contact point. The black double arrow line of 60 mm Φ represents the width of icing, which is larger than the diameter of the cylinder.

Calaghan P.T., R. Dykstra, C.D. Eccles, T.G. Haskell and J.D. Seymour (1999): A nuclear magnetic resonance study of Antarctic sea ice brine diffusivity. *Cold Reg Sci Tech*., **29**, 153–171: doi.org/10.1016/S0165-232X(99)00024-5.

Dehghani, S.R., Y.S. Muzychka and G.F. Naterer (2017): Water breakup phenomena in wave-impact sea spray on a vessel. *Ocean Eng*, **134**, 50-61: doi.org/10.1016/j.oceaneng.2017.02.013.

Dehghani, S.R., G.F. Naterer and Y.S. Muzychka (2018): 3-D trajectory analysis of wave-impact sea spray over a marine vessel. *Cold Reg. Sci. Tech.*, **146**, 72-80: doi.org/10.1016/j.coldregions.2017. 11.016.

Edelstein, W.A. and E.M. Schulson (1991): NMR imaging of salt-water ice. *J. Glaciol.*, **37**, 177–180: doi.org/10.3189/S0022143000042933.

Eicken, H, C. Bock, R. Wittig, H. Miller and H.O. Poertner (2000): Magnetic resonance imaging of sea-ice pore fluids: methods and thermal evolution of pore microstructure. *Cold Reg. Sci. Technol.*; **31**: 207–225: doi.org/10.1016/S0165-232X(00)00016-1.

Kawamura, T. (1988): Observations of the internal structure of sea ice by X ray computed tomography. *J. Geophys. Res*. **93**(C3), 2343–2350: doi:10.1029/jc093ic03p02343.

Kulyakhtin, A. and A. Tsarau (2014): A time-dependent model of marine icing with application of computational fluid dynamics. *Cold Reg. Sci. Tech.*, 104-105, 33-44: doi.org/10.1016/j.coldregions.2014.05.001.

Lozowski, E.P., K. Szilder and L. Makkonen (2000): Computer simulation of marine ice accretion. *Phil. Trans. R. Soc. Lond.*, **A358**, 2811–2845.

Makkonen, L. (1987): Salinity and growth rate of ice formed by sea spray. *Cold Reg. Sci. Tech*., **14**, 163–171.

Menzel M.I., S. Han, S. Stapf and B. Blümich (2000): NMR characterization of the pore structure and anisotropic self-diffusion in salt water ice. *J. Magn. Reson.*, **143**: 376–381: doi.org/10.1006/jmre.1999.1999.

Obbard, R.W., G. Troderman and I. Baker (2009): Imaging brine and air inclusions in sea ice using micro-X-ray computed tomography. *J. Glaciol*., **55,** 1113–1115: doi.org/10.3189/002214309790794814

Overland, J.E. (1990): Prediction of Vessel Ising for Near-Freezing Sea Temperature. *Weather and Forcasting*, **5**, 62-77.

Ozeki, T., K. Kose, T. Haishi, S. Nakatsubo and Y. Matsuda (2005): Network images of drainage channels in sea spray icing by MR microscopy. *Mag. Res. Imag*., **23**, 333-335.

Ozeki, T., H. Shimoda, D. Wako, S. Adachi and T. Matsuzawa (2013): Laboratory experiments of saline water spray icing - Features of hydrophilic and hydrophobic pliable sheets. *Proc. Int. Workshop on Atmospheric Icing of Structure 2013*, 5pp.

Ozeki, T., T. Matsuzawa, S. Adachi, T. Tokudome, T. Nunokawa, Y. Matsuda and A. Konno (2022): Laboratory experiment of spray icing using urea-doped water – Shape and amount of icing on cylindrical specimen with different diameters. *Proc. 36th Int. Symp. Okhotsk Sea and Polar Oceans*, 4pp.

Summary in Japanese

和文要約

尿素水を用いた平板試験体及び円筒試験体への飛沫着氷実験

尾関俊浩[1], 松沢孝俊[2], 野村慎吾[1], 安達聖[3], 徳留大樹[4],金野祥久[4]

[1]北海道教育大学札幌校, [2]海上技術安全研究所, [3]防災科研雪氷防災研究センター,[4]工学院大学

平板および円筒形の試験体を用いて，尿素を添加した飛沫着氷試験を行った．円筒試験体は直径 60, 165, 520 mm Φの 3 種類を用いた．平板試験体は風向に正対するように設置して着氷試験を行った．風速は 2 モード，噴霧粒子径は 3 種類を用いた．直径 165, 520 mm Φの試験では，衝突した噴霧の約半分が凍結した．60 mm Φでは着氷率が 50%より明らかに大きかった．一方，グラフデータ解析から得られた着氷断面積の増加量は，直径 520mm の円柱で大きく，直径 165mm の円柱で小さくなった．この結果は，試験体に成長した飛沫着氷の水平断面が，直径が小さくなるにつれて楕円形から逸脱することを示唆している．平板の着氷率をその幅にあたる 1000 mm に相当させてプロットした．対数近似の決定係数は 0.77 であり，良い一致が見られた．

Correspondence to: Toshihiro Ozeki,
ozeki.toshihiro@s.hokkyodai.ac.jp